Evidence of extreme type-III band offset at buried n-type CdO/p-type SnTe interfaces

M. J. Wahila, Z. W. Lebens-Higgins, N. F. Quackenbush, J. Nishitani, W. Walukiewicz, P.-A. Glans, J.-H. Guo, J. C. Woicik, K. M. Yu, and L. F. J. Piper

Phys. Rev. B **91**, 205307 — Published 18 May 2015

DOI: 10.1103/PhysRevB.91.205307

Evidence of extreme type III band offset at buried *n*-type CdO / *p*-type SnTe interfaces

M. J. Wahila,[1] Z. W. Lebens-Higgins,[1] N. F. Quackenbush,[1] J. Nishitani,[2,3] W. Walukiewicz,[2] P.-A. Glans,[4] J.-H. Guo,[4] J. C. Woicik,[5] K. M. Yu,[2,6] and L. F. J. Piper[1,*]

[1] *Department of Physics, Applied Physics and Astronomy, Binghamton University, Binghamton, New York 13902, USA*
[2] *Materials Sciences Division, Lawrence Berkeley National Laboratory, Berkeley, California 94720, USA*
[3] *Institute for Solid State Physics, The University of Tokyo, 5-1-5 Kashiwanoha, Kashiwa-shi, Chiba, 277-8581, Japan*
[4] *Advanced Light Source, Lawrence Berkeley National Laboratory, Berkeley, California 94720, USA*
[5] *Materials Science and Engineering Laboratory, National Institute of Standards and Technology, Gaithersburg, Maryland 20899, USA*
[6] *Department of Physics and Materials Science, City University of Hong Kong, Kowloon, Hong Kong SAR, China*

At covalent semiconductor interfaces, the band alignment is determined by the location of the band edges with respect to the charge neutrality level, but extension of this method to more ionic semiconductor systems requires further consideration. Using the charge neutrality level concept, a type III (or broken band gap) band offset is predicted at the interface between *n*-type CdO and *p*-type SnTe. Employing hard x-ray photoelectron spectroscopy, we report on the chemical composition at the buried interface and the valence band offset. Chemical intermixing at the interface between SnTe and CdO is found to be limited to ∼2.5 nm in our heterojunction samples. We measure a valence band offset of 1.95 (± 0.15 eV) irrespective of the layer configuration. Once the degenerate hole doping of the SnTe is considered, the measured band edge offset agrees with the type III offset predicted from alignment of the band edges with respect to the charge neutrality level of the semiconductors.

PACS numbers: 73.61.Ga, 79.60.Jv, 79.60.Dp, 68.35.Dv

I. INTRODUCTION

An accurate description of the energy band alignment at a semiconductor interface is vital because the interface defines the device properties[1,2]. Energetic alignment for covalent semiconductors, e.g. Si and GaAs, can be determined via work function alignment as a result of Fermi level pinning at the interface. The Fermi level pinning mechanism observed at traditional covalent semiconductor (group IV and III-V) interfaces is understood in terms of the energetic location of the charge neutrality level (CNL) or Fermi stabilization energy of the semiconductors[3–5].

At the semiconductor interface, evanescent in-gap states from the semiconductors are allowed to exist and enable charge-transfer that determines the energetic alignment. The character of these interfacial gap states, whether donor-like or acceptor-like, depends upon their energetic location with respect to the valence and conduction bands of the bulk material. The CNL (or branch-point energy) reflects the crossover between mostly acceptor-like to mostly donor-like states[6], thereby dictating the Fermi level pinning positions of covalent semiconductors[3–5]. As a result, plotting the energetic locations of the band edges with respect to the CNL can serve as a natural band alignment.

Energy alignment within more ionic systems can be more complex. Nevertheless, the CNL concept has been extended theoretically to describe the energy alignment at III-V and III/II oxide[7], and metal/organic semiconductor interfaces[8,9]. In addition, the location of the CNL has been employed to explain the electron accumulation observed at most *n*-type transparent conducting oxide surfaces, e.g. CdO[10], In_2O_3[11], ZnO[12], and SnO_2[13]. These findings suggest that the CNL concept could be used to direct the rational design of tailored interfaces for specific applications, e.g. modulation-doped heterojunctions for efficient charge separation[14].

To determine whether the CNL model could be employed to develop modulation-doped heterojunctions, we have examined the rocksalt/rocksalt heterojunction of *p*-type SnTe and *n*-type CdO. These two semiconductors represent extreme ends of the spectrum, exhibiting either extremely large electron or extremely large hole accumulation at their respective surfaces[10,15]. The resulting CdO/SnTe heterojunction thus displays interesting transport properties. These include a switchover from *n*-type to *p*-type with variation in SnTe film thickness, and a significant improvement of CdO electron mobility at the interface with SnTe[16]. These properties are believed to result from a large type III (or broken band gap) offset at the interface associated with the alignment of the band edges with respect to the CNL[16]. Direct evidence of the band alignment is required to confirm whether or not a type III interface originates from the Fermi level pinning at the respective CNL locations of the two semiconductors.

We have employed hard x-ray photoemission spectroscopy to determine the valence band offset at buried CdO/SnTe interfaces, i.e. 5 nm - 10 nm deep. X-ray

photoelectron spectroscopy provides a sensitive probe for measuring the energetic alignment at interfaces by directly measuring the valence band offset, but it is often restricted by its extremely surface sensitive nature. Progress in the development and application of HAXPES in the last decade has enabled studies of the valence band offset of buried interfaces[17–19]. Using an effective probing depth of 15 nm, we are able to distinguish between bulk, surface, and interfacial chemical contributions, and accurately determine the valence band offset. An extremely large type III band offset of 1.95 ± 0.15 eV was measured, in agreement with ~ 2.2 eV expected from aligning the known CNL locations of CdO and SnTe once the degenerate hole doping of the SnTe is considered.

II. EXPERIMENTAL DETAILS

Thin films of CdO and SnTe single layers and CdO/SnTe heterojunctions were deposited on glass substrates at 300°C using RF magnetron sputtering with an argon background pressure of 5 mTorr. The heterojunctions were fabricated by sequentially switching the RF power of the CdO and SnTe targets. The resulting heterojunctions were composed of either a single CdO layer on top of a single SnTe layer, or vice versa.

Film thicknesses ranged from 5 to 30 nm for single layer thin films, and 1 to 70 nm for layers within the CdO/SnTe heterojunctions. Film thicknesses were determined via Rutherford backscattering (RBS). The transport properties of the thin films were determined from Hall measurements in the van der Pauw geometry with a 0.6 T magnet. The optical absorption coefficients of CdO single layers were calculated using transmission and reflection measurements from a photospectrometer in the wavelength range of 250 to 2500 nm.

In addition, hard x-ray photoemission spectroscopy (HAXPES) and x-ray absorption spectroscopy (XAS) were performed at national synchrotron facilities to investigate both the films' occupied and unoccupied density of states. HAXPES can be used to probe both the core and valence occupied total density of states of a sample. Oxygen K-edge XAS, which utilizes transitions between the occupied O 1s core-level and the unoccupied hybridized O 2p states, only probes the unoccupied O 2p states within the conduction band.

HAXPES measurements were performed at the National Institute of Standards and Technology (NIST) bending magnet beamline X24 at the National Synchrotron Light Source (NSLS) at Brookhaven National Laboratory. Measurements were performed using a photon energy, $h\nu$, of 4 keV and a pass energy of 500 eV, with a corresponding Gaussian instrumental broadening of 0.45 eV. The binding energy axes were referenced to the Au $4f_{7/2}$ peak and Fermi edge of an Au foil in electrical contact with the film. To account for variations in photon flux, sample conductivity, and other factors, the spectral intensities were normalized with respect to the secondary electron intensity in regions away from the core-level or valence band region of interest. The take-off angle was 85° to increase its bulk sensitivity. The effective attenuation length, λ, was determined to be 5 nm from previous thickness-dependent studies, with $\sim 95\%$ of our signal coming within 3λ (15 nm) consistent with Dallera *et al.,* for the photon-energy used[17].

O K-edge XAS measurements were performed at the Advanced Light Source (ALS) using the ISAAC endstation at beamline 6.3.1. The XAS spectra were recorded in the surface-sensitive total electron yield (TEY) mode with an effective beamline resolution of 0.2 eV. To account for beam irregularities, the absorption signal was divided by the signal from a reference Au-coated mesh (I_0) in the incident photon beam. The spectral intensities were then normalized for easier comparison of spectral features.

Our previous studies have indicated that TEY mode XAS is sensitive to only the topmost 4 nm[20]. As a result, the TEY XAS only probes the same topmost layers as the effective attenuation length of our HAXPES, i.e. the portion of the samples from which $\sim 63\%$ of the HAXPES signal originates. As such, XAS was performed promptly after receiving the samples from the growers in order to reduce spectral contamination from exposure related surface compounds. Following those measurements, the samples were then stored in vacuum sealed bags until HAXPES was performed.

A. Optoelectronic properties of CdO

Three CdO thin film samples of varying thicknesses were experimentally examined. Optical band gaps were determined using Tauc plots of $(\alpha h\nu)^2$ versus energy, shown in Figure 1 (a). By fitting a line to the absorption edges observed in the Tauc plots, the optical band gap is given by the x-intercept corresponding to the onset of optical absorption.

In addition, valence band leading edges were extrapolated from HAXPES measurements, shown in Figure 1 (b). The valence band leading edges were determined for each film by fitting both the flat, unoccupied region above the Fermi level and the main valence band edge with lines. The intercept of the two lines gives the onset energy of the valence band leading edge with respect to the Fermi level.

With increasing film thickness, there is a clear decrease in the optical band gap from 2.88 eV to 2.69 eV and in the valence band leading edge from 1.79 eV to 1.29 eV. However, our O K-edge XAS spectra of the CdO films ≥ 5 nm, shown in Figure 1 (c), display little to no differences between films and are consistent with previously reported spectra from bulk CdO[21].

The carrier statistics for these films were modeled using a non-parabolic conduction band dispersion, which has been widely used for CdO films with high carrier concentrations[22,23]. The non-parabolic conduction band

	RBS	Hall			HAXPES	Optical
	Thickness (nm)	Type	n (cm^{-3})	Mobility ($cm^2/V{\cdot}s$)	VB_{LE} (eV)	E_g^{opt} / E_g^{model} (eV)
CdO	5	N	2.44×10^{20}	30.35	1.79	2.88 / 2.52
	10	N	3.069×10^{20}	56.04	1.52	2.76 / 2.58
	20	N	3.24×10^{20}	73.9	1.27	2.69 / 2.59
SnTe	5 → 30	P	$4.32 \rightarrow 1.744 \times 10^{21}$	5.276 → 15.92	(-0.26 – -0.46)	(–/–)

TABLE I. Table includes approximate thicknesses from RBS; carrier type, concentration, and mobility from Hall measurements; valence band leading edge binding energies from HAXPES; and optical band gaps from experimental measurements and theoretical modeling. Optical gaps of SnTe were not examined due to equipment limitations.

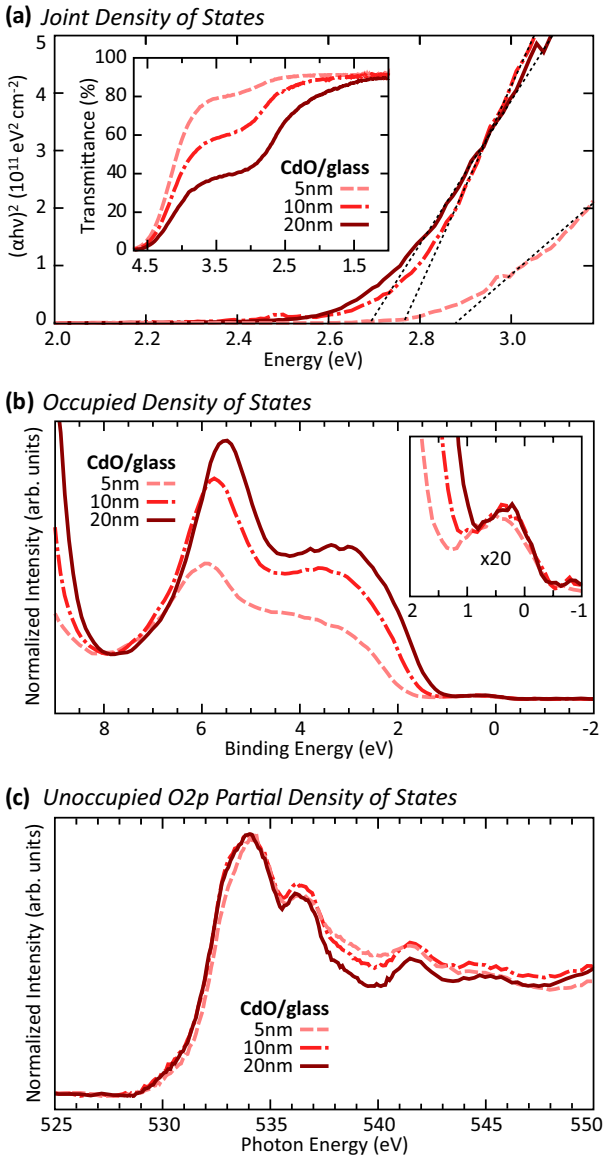

FIG. 1. (a) Tauc plot analysis of the direct band gap absorption onset for CdO films of varying thickness (transmission spectra inset). (b) HAXPES valence band spectra of CdO films showing Fermi level shifting correlated to film thickness (magnified Fermi edge inset). (c) O K-edge XAS of CdO films.

dispersion, due to the interaction between the conduction and valence bands, is given by

$$E_C(k)\left(1+\frac{E_C(k)}{E_g}\right)=\frac{\hbar^2k^2}{2m_0^*}, \quad (1)$$

which is dependent on experimentally determined parameters: the direct band gap E_g, and the conduction band edge effective mass m_0^*. An E_g of 2.16 eV and an m_0^* value of $0.21m_0$ at the Γ point were used for these calculations[23].

We have accounted for conduction band renormalization effects with a model that has demonstrated significant success for InN[24]. We have included both electron-electron ($\Delta E_{e\cdot e}$) and electron-ion interactions ($\Delta E_{e\cdot i}$)[24,25] as follows:

$$E_g' = E_g + \Delta E_{e\cdot e} + \Delta E_{e\cdot i}, \quad (2)$$

The renormalization due to electron-electron interactions is given by

$$\Delta E_{e\cdot e} = -\frac{2e^2k_F}{\pi\varepsilon_s} - \frac{e^2k_{TF}}{2\varepsilon_s}\left[1-\frac{4}{\pi}\arctan\left(\frac{k_F}{k_{TF}}\right)\right], \quad (3)$$

where $k_F = (3\pi^2 n)^{1/3}$ is the Fermi wave vector, $k_{TF} = (2/\sqrt{\pi})(k_F/a_0)^{1/2}$ is the Thomas-Fermi screening wave vector, $a_0 = \varepsilon_s\hbar^2/m_F^*e^2$ is the effective Bohr radius, ε_s is the static dielectric constant, and m_F^* is the effective mass at the Fermi level in the conduction band.

The renormalization due to electron-ion interactions is then given by

$$\Delta E_{e\cdot i} = -\frac{4\pi n e^2}{\varepsilon_s a_0 k_{TF}^3}. \quad (4)$$

An ε_s value of $21.9\varepsilon_0$ was used to calculate the renormalization components[22].

The results of the experimental measurements and theoretical modeling are compiled in Table I. For a carrier concentration of 3×10^{20} cm^{-3}, similar to that of our CdO films, the Fermi level is expected to lie about 2.57 eV above the valence band at the Γ point due to the combination of non-parabolic conduction band filling and band

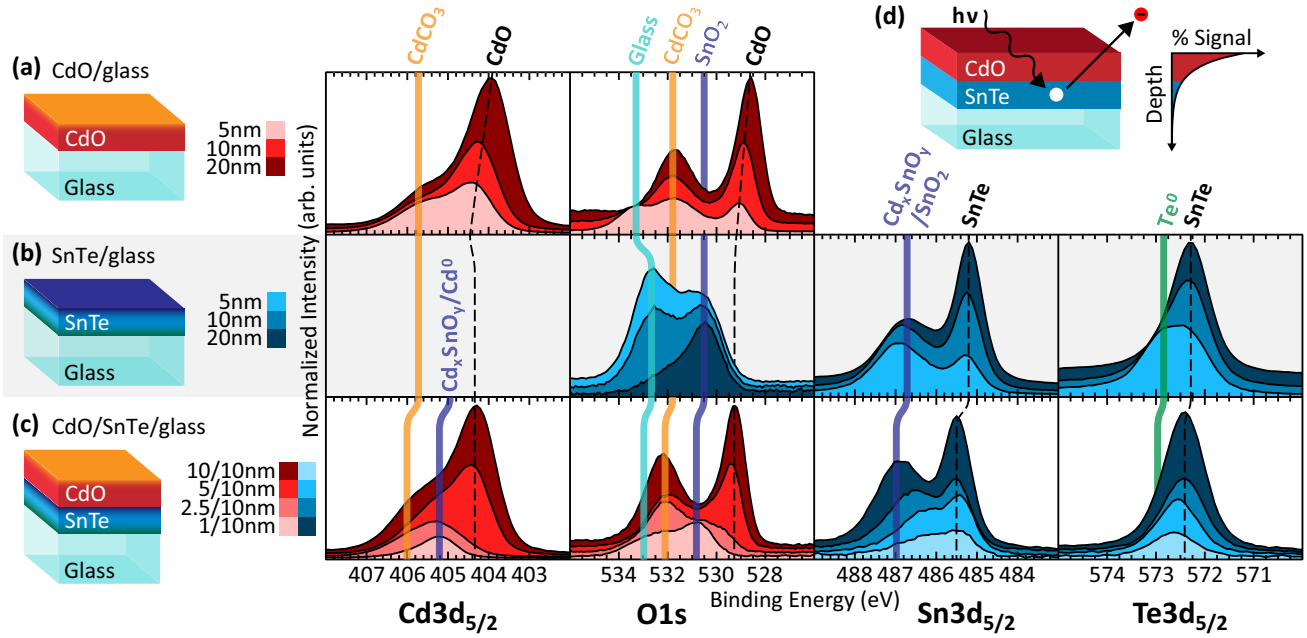

FIG. 2. Schematic diagrams and HAXPES Cd $3d_{5/2}$, O 1s, Sn $3d_{5/2}$, and Te $3d_{5/2}$ core-level peaks for series of varying thickness (a) CdO thin films, (b) SnTe thin films, and (c) CdO films on top of SnTe films, all grown on slide glass substrate. Vertical dotted lines identify peaks corresponding to bulk charge states, while the thicker lines identify surface and interface species. Contamination/intermixing lines are color-coded to match the surface/interface they are attributed to in the sample schematics on the left. (d) A diagram showing the exponential drop-off of HAXPES spectral contributions from within a sample.

gap shrinkage. However, the measured optical band gaps for all three CdO samples are larger than what is expected from band filling alone.

For uniform degenerate doping, a direct relationship between the carrier concentration and Fermi level position is expected due to a Moss-Burstein shift. However, as shown by the shifting valence band spectra of Figure 1 (b), the CdO thin films display a thickness dependent Fermi level shift which is characteristic of an inhomogeneous carrier concentration within the films. A similar relationship between carrier concentration and film thickness was observed for InN due to a combination of surface and interface charge accumulation[26]. As such, we attribute the degenerate filling observed above the main valence band edge of our CdO primarily to electron accumulation at the surface and interface.

A summary of the experimental results for SnTe thin films is also included in Table I. We note that each of the examined SnTe films had a *p*-type carrier concentration greater than 10^{21} cm^{-3}. This high *p*-type carrier concentration suggests that the Fermi level will lie approximately 0.5 eV below the valence band maximum in our SnTe films[15]. This is supported by our valence band leading edge measurements, which confirm the occupied valence states extend up to the Fermi level. Additionally, the SnTe optical absorption onset was below the range of our optical apparatus, precluding optical band gap measurements on SnTe films.

B. Chemical intermixing at CdO/SnTe interfaces

Before investigating the valence band offsets of the heterojunctions, the quality of the interfaces was established. The heterojunctions were examined to determine if mixed phases or contamination existed, resulting in a non-abrupt interface. Interface properties for the III-V system have been widely investigated with XPS and various other techniques revealing evidence of ion exchange reactions and clustering[27,28]. XPS studies examining CdO and SnTe single layers have identified the formation of surface oxides upon exposure to atmospheric gases. Examination of SnTe after exposure to molecular oxygen indicated a large increase in Sn^{4+} with the rapid formation of surface SnO_2, as well as a small increase in additional Te charge states[29,30]. Additionally, various oxide (and or carbonate) species have been shown to form on the CdO surface, but can be mostly removed upon annealing[31,32].

The results of the surface and interface investigation performed on the CdO and SnTe thin films are detailed in Figure 2. Taking advantage of the exponential decay of the HAXPES signal with depth, depicted in Figure 2 (d), atomic core-level peaks were assigned to either the film surface, bulk, or buried interface by examining films of varying thicknesses. Core-level peaks were attributed to the film surface if their contribution stayed relatively constant between all film thicknesses. Peaks were attributed to the buried interface if they only appeared once the top film thickness became comparable to the probing depth

of the HAXPES, and their contribution then increased with decreasing film thickness. And finally, peaks were attributed to the bulk if they were present in varying degrees for all or most of the film thicknesses. Comparing the binding energies of these core-level peaks to literature values[29,31] then allowed for the identification of surface, bulk, and interfacial compounds.

Figure 2 (a) and (b) show core-level HAXPES spectra for 5, 10, and 20 nm thick films of CdO and SnTe, respectively. These films were used to characterize the quality of the film growth and identify the compounds that form on the film surfaces and at the substrate interface. It was determined that oxides such as $CdCO_3$ exist on the exposed CdO film surfaces, but no discernible intermixing occurs between the CdO and glass substrate. The SnTe films, however, show compounds at both interfaces, with SnO_2 at the film surface and what is likely metallic Te at the glass interface. Both of these findings are consistent with previous studies of surface oxidation and contamination of CdO[31,32] and SnTe[29,30].

Figure 2 (c) shows the core-levels for 1, 2.5, 5, and 10 nm films of CdO grown on top of 10 nm of SnTe. Similar to the CdO reference films, $CdCO_3$ contamination is found to exist on the exposed CdO surface; however, an additional peak, likely due to Cd_xSnO_y or metallic Cd[33,34], is observed in the Cd 3d region and is attributed to the heterojunction interface. Additionally, a second Sn 3d peak, likely Cd_xSnO_y or SnO_2[29,33], is also attributed to the heterojunction interface. These peaks indicate film intermixing at the interface resulting in mixed Cd/Sn oxides.

While comparable intermixing was found in both heterojunction configurations, the exact chemical species and texture of the interface intermixing may differ between CdO grown on SnTe and SnTe grown on CdO. This could account for the differences in the electronic transport properties between heterojunction configurations[16]. For example, switching the film order for a 10nm/10nm heterojunction resulted in a four-fold increase in carrier concentration, but a decrease in mobility (see Table II). However, determining the effects of intermixing on electronic transport properties is beyond the scope of this study.

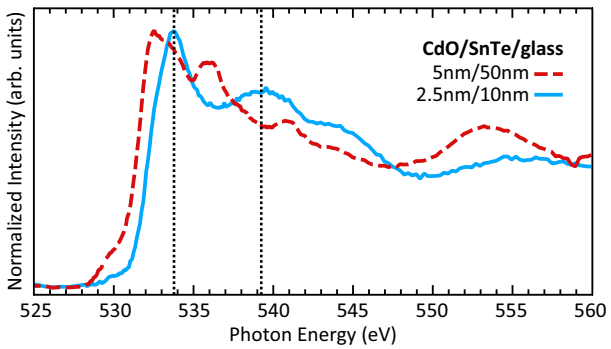

FIG. 3. XAS of two samples of CdO on SnTe. Vertical dotted lines correspond to features indicative of SnO_2[35].

Our HAXPES results are supported by our O K-edge XAS measurements for CdO on SnTe heterojunction samples, shown in Figure 3. By comparison to XAS spectra previously reported in the literature, we find that samples with $\geq$ 5 nm films of CdO compare well with bulk CdO[21], while CdO films $\leq$ 2.5 nm display noticeable contributions from what is most likely SnO_2 at the heterojunction interface[35]. These results are consistent with our HAXPES analysis, where we conclude some tin oxide compounds must exist at the heterojunction interface.

This analysis puts limits on the heterojunction film thicknesses that we can reasonably investigate further. The probing depth of our HAXPES measurements limit the topmost film thickness to $\lesssim$ 10 nm in order to observe the buried heterojunction interface. In addition, the surface and interfacial compounds place a lower limit of $\geq$ 2.5 nm on film thickness, as the surface and interfacial compounds dominate in thinner films.

C. Valence band offset of CdO/SnTe interfaces

Nine different heterojunction samples were examined further, including both CdO on SnTe and SnTe on CdO. All nine samples had CdO layers $\geq$ 5 nm and SnTe layers $\geq$ 10 nm, i.e. limited surface and interfacial contributions. Due to spectral overlap in the valence band region of our HAXPES measurements, the valence band offset between CdO and SnTe (ΔVBO)[36] was determined via core-level offsets as follows:

$$\Delta VBO = E^{HJ}_{\Delta CL} + (\Delta CdO^{Bulk}_{CL-LE}) - (\Delta SnTe^{Bulk}_{CL-LE}), \quad (5)$$

where $E^{HJ}_{\Delta CL}$ is the energy difference between a SnTe and CdO core-level within a heterojunction, $(\Delta CdO^{Bulk}_{CL-LE})$ is the energy difference between a reference bulk CdO core-level and valence band leading edge, and $(\Delta SnTe^{Bulk}_{CL-LE})$ is the difference between a reference bulk SnTe core-level and leading edge of the bulk SnTe occupied valence states. Figure 4 (a) depicts the method for determining the core-level to leading edge separations for reference bulk CdO and SnTe films.

Three SnTe core-levels (Sn $3d_{5/2}$, Te $3d_{5/2}$, and Sn $4d_{5/2}$) were used in conjunction with the CdO Cd $3d_{5/2}$ core-level to determine $E^{HJ}_{\Delta CL}$ for each heterojunction sample. An example of this method for a heterojunction of each layer configuration, i.e. CdO on SnTe and SnTe on CdO, is shown in Figure 4 (b). The valence band offsets determined using each of the three SnTe core-levels were comparable, with no changes due to the overall shifts in binding energy of the CdO and SnTe single layer thin films. We obtain an offset of 1.95 ± 0.15 eV irrespective of layer configuration. Experimental offsets for individual heterojunction samples are given in Table II. The experimental results are summarized in Figure 5.

Configuration	Thickness (nm)	Type	n (cm^{-3})	Mobility ($cm^2/V{\cdot}s$)	Offset (eV)
SnTe/CdO	10 / 10	N	9.17×10^{20}	18.1	1.98
	10 / 20	N	4.92×10^{20}	36.58	1.72
	10 / 5	N	2.55×10^{21}	6.352	2.03
CdO/SnTe	10 / 10	N	2.46×10^{20}	30.56	1.74
	5 / 10	N	1.94×10^{20}	24.25	1.91
	5 / 20	N	1.80×10^{20}	20.75	2.04
	5 / 30	N	2.53×10^{20}	13.12	2.07
	5 / 60	P	2.03×10^{21}	2.051	1.98
	5 / 70	P	7.10×10^{20}	4.956	2.09

TABLE II. Characterization of CdO/SnTe heterojunctions, including electronic transport properties from Hall measurements and experimentally determined valence band offsets.

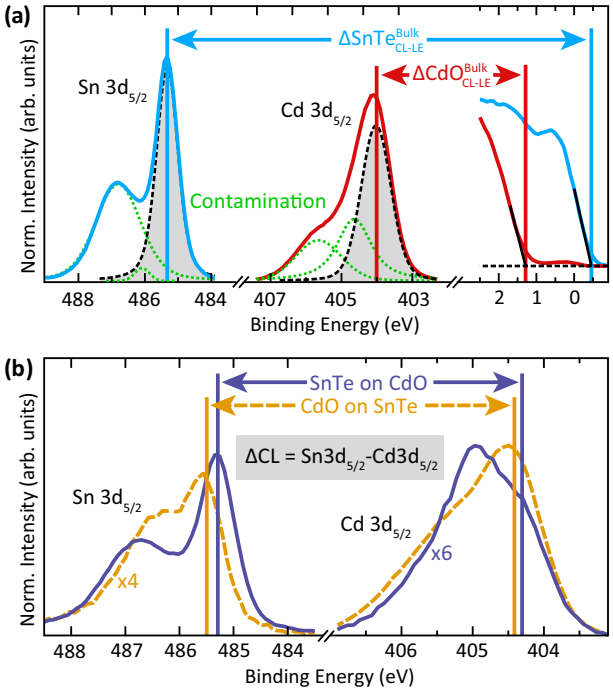

FIG. 4. (a) The method for determining the energy separation between a core-level and valence band leading edge for example bulk SnTe and bulk CdO thin films, and (b) the difference between a SnTe and a CdO core-level for two example heterojunctions.

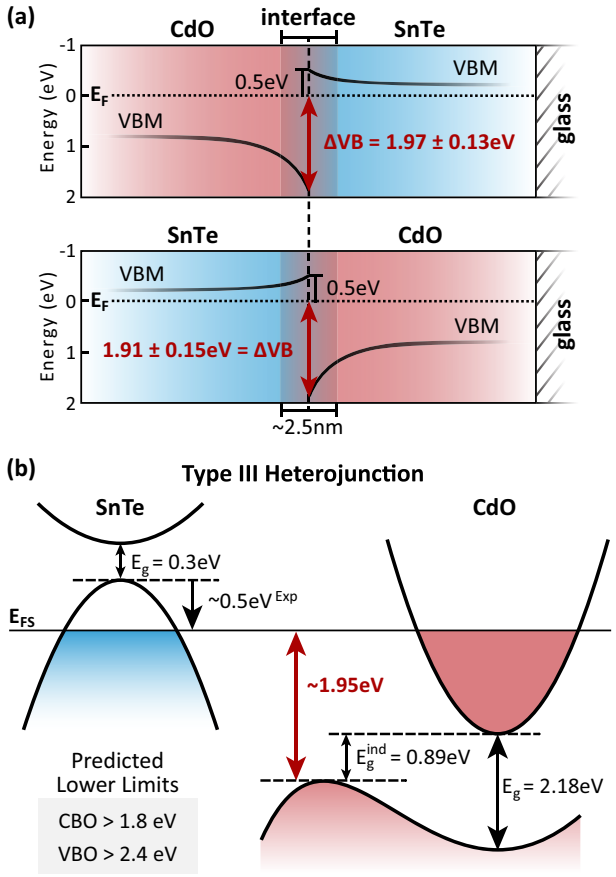

FIG. 5. (a) Diagram of the band bending at the interface for CdO on SnTe (top) and SnTe on CdO (bottom) heterojunction configurations. ΔVB is the experimentally determined offset between the valence band of CdO and Fermi level at the interface. (b) Simplistic diagram of the valence and conduction bands at the heterojunction interface, based on our experimental band offsets. Band gap values for CdO and the CNL location for SnTe were obtained from theoretical calculations[37] and ion irradiation studies[15], respectively.

The large valence band offset results in an extreme type III discontinuity, with the CdO conduction band minima (CBM) lying $\sim$ 1.5 eV below the valence band maxima (VBM) of SnTe.

Our measured values are consistent with those predicted from the alignment of the band edges to a universal CNL. Based on ion irradiation studies, the CNL of CdO is expected to lie around 1 eV above the CBM corresponding to a carrier concentration of $5{\times}10^{20}$ cm^{-3}[38], in good agreement with ARPES studies of the electron accumulation[10]. Recent hybrid density functional theory calculations similarly locate the CNL 1.26 - 1.43 eV above the CBM of CdO (or 2.15 - 2.32 eV above the VBM)[37], in relative agreement with 2.45 eV above the

VBM from quasiparticle calculations[7]. Fewer studies exist for SnTe, however, the CNL has been located at 0.5 eV below the SnTe VBM with a high carrier concentration around 3×10^{21} cm^{-3}[15].

Alignment of the aforementioned CNL energies for CdO and SnTe results in VBM offsets ranging from 2.39 to 2.82 eV. Accounting for the degenerate hole doping in SnTe, i.e. pinning the Fermi level at the CNL ∼0.5 eV below the VBM of SnTe, yields a predicted valence band offset of 1.89 - 2.32 eV. This predicted offset is consistent with our measured value of 1.95 ± 0.15 eV, and is an indication of the extreme type III interface between our CdO and SnTe thin films.

III. CONCLUSION

Using hard x-ray photoelectron spectroscopy and films with limited chemical intermixing at the interface, we determined an effective valence band offset of 1.95 (± 0.15 eV) irrespective of layer configuration of the CdO/SnTe heterojunctions. Our measurements are in good agreement with the expected offset from CdO and SnTe CNL alignment, once the degenerate hole doping of the SnTe is considered. A pronounced type III band offset is therefore confirmed to exist at this interface, with the CdO CBM lying ∼ 1.5 eV below the VBM of SnTe. This type III interface is likely responsible for the remarkable transport properties, which include a transition from p-type to n-type at these dimensions and enhanced electron mobility at the interface. Our work suggests that other extreme modulation-doped heterojunctions could be designed through consideration of the natural band alignment of oxide semiconductors from knowledge of their CNL energetic locations.

IV. ACKNOWLEDGMENTS

L. F. J. P. and N. F. Q. acknowledge support from the National Science Foundation under DMR 1409912. Z. W. L.-H. is grateful for an undergraduate Summer Scholars and Artists Award from Binghamton University. This work was supported by the Director, Office of Science, Office of Basic Energy Sciences, Materials Sciences and Engineering Division, of the U.S. Department of Energy under Contract No. DE-AC02-05CH11231. The Advanced Light Source is supported by the Director, Office of Science, Office of Basic Energy Sciences, of the U.S. Department of Energy under contract no. DE-AC02-05CH11231. Use of the National Synchrotron Light Source at Brookhaven National Laboratory was supported by the U.S. Department of Energy, Office of Science, Office of Basic Energy Sciences, under Contract No. DEAC02-98CH10886. Beamline X24a is supported by the National Institute of Standards and Technology.

* lpiper@binghamton.edu

[1] H. Kroemer, Jpn. J. Appl. Phys. **20**, 9 (1981).
[2] H. Lüth, *Solid Surfaces, Interfaces and Thin Films* (Springer Berlin Heidelberg, Berlin, 2001).
[3] J. Tersoff, Phys. Rev. B **32**, 6968(R) (1985).
[4] W. Walukiewicz, Phys. Rev. B **37**, 4760 (1988).
[5] W. Mönch, *Electronic Properties of Semiconductor Interfaces* (Springer, Berlin, 2004).
[6] L. F. J. Piper, T. D. Veal, M. J. Lowe, and C. F. McConville, Phys. Rev. B **73**, 195321 (2006).
[7] A. Schleife, F. Fuchs, C. Rödl, J. Furthmüller, and F. Bechstedt, Appl. Phys. Lett. **94**, 012104 (2009).
[8] H. Vázques, Y. J. Dappe, J. Ortega, and F. Flores, J. Chem. Phys. **126**, 144703 (2007).
[9] J. O. F. Flores and H. Vázquez, in *Advances in Solid State Physics, Volume 48*, edited by R. Haug (Springer Berlin Heidelberg, Berlin, 2009).
[10] L. F. J. Piper, L. Colakerol, P. D. C. King, A. Schleife, J. Zúñiga-Pérez, P. a. Glans, T. Learmonth, A. Federov, T. D. Veal, F. Fuchs, et al., Phys. Rev. B **78**, 165127 (2008).
[11] P. D. C. King, T. D. Veal, D. J. Payne, A. Bourlange, R. G. Egdell, and C. F. McConville, Phys. Rev. Lett. **101**, 116808 (2008).
[12] L. F. J. Piper, A. R. H. Preston, A. Fedorov, S. W. Cho, A. DeMasi, and K. E. Smith, Phys. Rev. B **81**, 233305 (2010).
[13] T. Nagata, O. Bierwagen, M. E. White, M. Y. Tsai, Y. Yamashita, H. Yoshikawa, N. Ohashi, K. Kobayashi, T. Chikyow, and J. S. Speck, Appl. Phys. Lett. **98**, 232107 (2011).
[14] A. C. G. R. Dingle, H. L. Stormer and W. Wiegmann, Appl. Phys. Lett. **33**, 7 (1978).
[15] J. Nishitani, D. Detert, J. Beeman, K. M. Yu, and W. Walukiewicz, Appl. Phys. Exp. **7**, 091201 (2014).
[16] J. Nishitani, K. M. Yu, and W. Walukiewicz, Appl. Phys. Lett. **105**, 132103 (2014).
[17] C. Dallera, L. Duó, L. Braicovich, G. Panaccione, G. Paolicelli, B. Cowie, and J. Zegenhagen, Appl. Phys. Lett. **85**, 4532 (2004).
[18] G. Conti, A. M. Kaiser, A. X. Gray, S. Nemšák, G. K. Pálsson, J. Son, P. Moetakef, A. Janotti, L. Bjaalie, C. S. Conlon, et al., Journal of Applied Physics **113**, 143704 (2013).
[19] A. M. Kaiser, A. X. Gray, G. Conti, B. Jalan, A. P. Kajdos, A. Gloskovskii, S. Ueda, Y. Yamashita, K. Kobayashi, W. Drube, et al., Appl. Phys. Lett. **100**, 261603 (2012).
[20] N. F. Quackenbush, J. W. Tashman, J. A. Mundy, S. Sallis, H. Paik, R. Misra, J. A. Moyer, J.-H. Guo, D. A. Fischer, J. C. Woicik, et al., Nano Letters **13**, 4857 (2013).
[21] L. F. J. Piper, A. DeMasi, K. E. Smith, A. Schleife, F. Fuchs, F. Bechstedt, J. Zuniga-Pérez, and V. Munoz-Sanjosé, Phys. Rev. B **77**, 125204 (2008).
[22] Y. Zhu, R. J. Medelsberg, J. Zhu, J. Han, and A. Anders, J. Phys. D: Appl. Phys. **46**, 195102 (2013).
[23] P. H. Jefferson, S. A. Hatfield, T. D. Veal, P. D. C. King, C. F. McConville, and V. Muñoz-Sanjosé, Appl. Phys. Lett. **92**, 022101 (2008).

[24] J. Wu, W. Walukiewicz, W. Shan, K. M. Yu, J. W. Ager III, E. E. Haller, H. Lu, and W. J. Schaff, Phys. Rev. B **66**, 201403(R) (2002).
[25] K.-F. Berggren and B. E. Sernelius, Phys. Rev. B **24**, 1971 (1981).
[26] L. F. J. Piper, T. D. Veal, C. F. McConville, H. Lu, and W. J. Schaff, Appl. Phys. Lett. **88**, 252109 (2006).
[27] E. Papis-Polakowska, J. Kaniewski, J. Szade, W. Rzodkiewicz, A. Jasik, K. Reginski, and A. Wawro, Thin Solid Films **522**, 223 (2012).
[28] M. Losurdo, P. Capezzuto, G. Bruno, A. Brown, T. Brown, and G. May, J. of Appl. Phys. **100**, 013531 (2006).
[29] V. S. Neudachina, T. B. Shatalova, V. I. Shtanov, L. V. Yashina, T. S. Zyubina, M. E. Tamm, and S. P. Kobeleva, Surface Science **584**, 77 (2005).
[30] S. Badrinarayanan, A. Mandale, and A. Sinha, Materials Chemistry and Physics **11**, 1 (1984).
[31] L. F. J. Piper, P. H. Jefferson, T. D. Veal, C. F. McConville, J. Zúñiga-Pérez, and V. Muñoz-Sanjosé, Supperlattices and Microstructures **42**, 197 (2007).
[32] J. J. Mudd, T.-L. Lee, V. Muñoz-Sanjosé, J. Zúñiga-Pérez, D. Hesp, J. M. Kahk, D. J. Payne, R. G. Egdell, and C. F. McConville, Phys. Rev. B **89**, 035203 (2014).
[33] T. Hashemi, C. Hogarth, and F. Golestani-Fard, Journal of Materials Science **23**, 2645 (1988), ISSN 0022-2461, URL `http://dx.doi.org/10.1007/BF01111927`.
[34] C. Powell, Journal of Electron Spectroscopy and Related Phenomena **185**, 1 (2012), ISSN 03682048, URL `http://linkinghub.elsevier.com/retrieve/pii/S0368204811001307`.
[35] M. Kapilashrami, C. X. Kronawitter, T. Törndahl, J. Lindahl, A. Hultqvist, W.-C. Wang, C.-L. Chang, S. S. Mao, and J. Guo, Phys. Chem. Chem. Phys **14**, 10154 (2012).
[36] K.-K. Lee, W. Priyantha, and T. H. Myers, Appl. Phys. Lett. **100**, 052108 (2012).
[37] M. Burbano, D. Scanlon, and G. Watson, J. Amer. Chem. Soc. **133**, 15065 (2011).
[38] D. T. Speaks, M. A. Mayer, K. M. Yu, S. S. Mao, E. E. Haller, and W. Walukiewicz, J. Appl. Phys. **107**, 113706 (2010).